Journal of Applied Polymer Science

Protein-imprinted polyurethane-grafted calcium alginate hydrogel microspheres

Lingxie Li, Xiaoguang Ying, Jiangquan Liu, Xiao Li, Weiying Zhang
Institute of Polymer Science and Engineering, College of Chemical Engineering, Fuzhou University, Fuzhou 350108, China
Correspondence to: X. Ying (E-mail: yxg@fzu.edu.cn)

ABSTRACT: Protein-imprinted polyurethane-grafted calcium alginate hydrogel microspheres were prepared and characterized. The samples were investigated with optical microscopy, scanning electron microscopy, ^{13}C-NMR, and Fourier transform infrared spectroscopy. We proved that polyurethane side chains were successfully grafted, and this led to a relatively rough and dense surface. The samples exhibited better swelling durability when applied in specific adsorption tests. The adsorption kinetic and recognition properties indicated that the imprinted modified microspheres had excellent rebinding affinity toward the target proteins. Moreover, the influence of the preassembly pH, rebinding pH, and grafting ratio on the adsorption capacity and imprinting efficiency (IE) were systematically investigated. The study results suggest that the modified samples possessed a higher IE toward the target protein under the optimum pH and grafting ratio. Upon polyurethane grafting modification, the alginate hydrogel microspheres showed improved mechanical stability and recognition specificity. © 2015 Wiley Periodicals, Inc. J. Appl. Polym. Sci. **2015**, *132*, 42140.

KEYWORDS: grafting; molecular recognition; polysaccharides; polyurethanes; proteins

Received 13 November 2014; accepted 13 February 2015
DOI: 10.1002/app.42140

INTRODUCTION

With the development of life sciences, the selective detection and quantification of target proteins have attracted much attention.[1] Biosensors have been reported previously to offer high selectivity toward target molecules, but they have shown low stability and have a high production cost.[2–4] To prevent these drawbacks, researchers have focused on the synthesis of artificial sensors that are capable of recognizing and binding desired molecules.

Molecularly imprinted polymers (MIPs), prepared by the copolymerization of monomers in the presence of a template molecule,[5] have been widely researched and successfully applied for the recognition of small molecules. Compared with that of small molecules, the imprinting of protein is developing relatively slowly. This is because their huge molecular size, flexible conformation, complex construction, and poor solubility in aqueous solvents cause difficulties in the imprinting process.

Considering these difficulties, a variety of approaches have been developed, for example, surface imprinting,[6] epitope imprinting,[7] and the use of novel materials, such as cryogels[8] and hydrogels.[9] Over the past decade, hydrogel-based protein-imprinted polymers have been well documented. Acrylamide and its derivatives have been commonly used as monomers to synthesize hydrophilic MIPs.[10] Protein-imprinted polyacrylamide hydrogels have been successfully used in chromatographic separation.[6,11] To find more applications in the fields of molecular imprinting, other monomers have been introduced, such as methyl methacrylate and *N*-isopropyl acrylamide.[12,13] However, most of these procedures have involved radical polymerization and were, therefore, challenged in protein configuration preservation and template reversible removal. With the aim of a more suitable imprinting environment for proteins, natural hydrogels, such as agarose, chitosan, and alginate, have been used recently.[14–16] Zhang *et al.*[17] and Herrero and coworkers[18,19] prepared bovine serum albumin (BSA) imprinted calcium alginate (CaA) hydrogel microspheres under mild circumstances. Zhao *et al.*[20] prepared BSA-imprinted CaA/phosphate hybrid microspheres. Ying *et al.*[21] used hydroxyethyl cellulose and sodium alginate (SA) to form interpenetrating networks for protein imprinting. The materials prepared previously showed good imprinting efficiency (IE) and specificity. However, their mechanical strength and swelling stability required improvement.

In this research, polyurethane-grafted calcium alginate (PU-*g*-CaA) was chosen as a protein-imprinting matrix. Grafted polyurethane (PU) side chains have been reported to improve the mechanical and chemical stability of hydrogels; this benefitted the recognition properties.[22] Moreover, the protein templates

in this procedure were protected from initiator radical denaturation because the grafting modification was performed before the addition of protein templates. The structure and morphology of the modified material were characterized, and influencing factors on the specific rebinding of protein were studied. These included the swelling properties and pH values in the preassembling and rebinding process.

EXPERIMENTAL

Materials

SA chemical pure was purchased from Shanghai Chemical Reagents Corp. Isophorone diisocyanate [analytical-reagent (AR) grade] was obtained from Three Trees Co., Ltd. (China). 2-Hydroxyethyl methacrylate (AR grade) and dimethylolpropionic acid (AR grade) were purchased from Shanghai Crystal Pure Reagent Co., Ltd. (China). BSA (pI = 4.7, molecular weight (M_w) = 66 kDa) and ovalbumin (OVA; pI = 4.7, M_w = 46 kDa) were supplied by Sigma-Aldrich. Tris(hydroxymethyl) aminomethane (AR grade) was purchased from Aladdin Industrial Corp.

Synthesis of PU-*g*-SA

Synthesis of PU-*g*-SA is a two-step procedure involving PU synthesis and grafting onto SA, which was introduced elsewhere[23] and is described briefly as follows. PU was prepared by the addition of a specified amount of isophorone diisocyanate and 2-hydroxyethyl methacrylate in a 125-mL three-necked flask followed by magnetic stirring at 35°C with dibutyltin dilaurate as a catalyst. When the content of isocyanate groups (NCO) was reduced by half, dimethylolpropionic acid was added, and the temperature was raised to 55°C. The reaction was allowed until NCO was not detectable. The grafting reaction was carried out under a nitrogen atmosphere in a 250-mL four-necked flask maintained at a constant temperature. SA was dissolved in deionized water and added to the flask. Then, the synthesized PU and redox initiator composed of $K_2S_2O_8$ and Na_2SO_3 were added dropwise. The polymerization was allowed to proceed for 4 h at 55°Cto obtain the PU-*g*-SA solution.

To calculate the grafting ratio, the PU-*g*-SA solution was gelated in a calcium chloride ($CaCl_2$) solution and extracted with acetone to remove the remaining reactants and homopolymers before the test. The grafting ratio (G%) was estimated according to eq. (1):

$$G\% = (W_1 - W_0)/W_0 \times 100 \quad (1)$$

where W_0 and W_1 are the weights of the original CaA and the grafted product, respectively. The grafting ratio was controlled by the variation of the added amount of synthesized PU during the grafting process.

Preparation of Protein-Imprinted Microspheres

Molecularly imprinted beads were produced by Ca^{2+} ionic crosslinking of the PU-*g*-SA solution in the presence of protein. The protein solution (2 mg/mL, 10 mL) was mixed with PU-*g*-SA, whose pH was adjusted to 4.1 by adding 0.1 mol/L hydrochloride solution, whereas in the preassembly study, the pH ranged from 3.8 to 4.9. Then, 0.2 g of SA was added to maintain the polymer concentration. The mixture was preassembled for 4 h, then dropped from an injector into a $CaCl_2$ aqueous solution (2% w/w), and gelated for 1 h to form hydrogel microspheres. The generated microspheres were placed in an Erlenmeyer flask containing 30 mL of eluant [a mixture of 1% $CaCl_2$ solution and 0.05M tris(hydroxymethyl) aminomethane/HCl buffer with a pH of 7.58], which was refreshed every 3 h. The concentration of protein was detected by an ultraviolet–visible spectrophotometer at 280 nm. This process was conducted at room temperature until no protein was detected in the eluant. Nonimprinted polymers (NIPs) were synthesized under the same conditions as reported previously, except for the absence of the protein template.

Rebinding Experiments

The adsorption kinetics of the prepared MIPs and NIPs was carried out as follows. Accurately weighed microspheres were incubated with a BSA solution. The concentration in the supernatant was detected every 5 min. The adsorption capacity (Q) was calculated with eq. (2):

$$Q = (C_0 - C_t)V/m \quad (2)$$

where C_0 and C_t are the initial and equilibrium concentrations of protein, respectively; V is the volume of protein solution; and m is the mass of the microspheres.

The IE was calculated with eq. (3):

$$\mathrm{IE} = Q_M/Q_N \quad (3)$$

where Q_M is the rebinding capacity of the protein on the imprinted microspheres and Q_N is the adsorption capacity of equally weighted nonimprinted microspheres.

Measurements

Fourier transform infrared (FTIR) spectra were recorded with an FTIR spectrometer (Spectrum-2000FTIR, PerkinElmer Corp.) from 400 to 4000 cm^{-1} under 25°C with KBr pellets. The ^{13}C-NMR spectra were obtained on an NMR spectrometer (Avance III500, Bruker Corp., Switzerland). The modified samples were extracted with acetone to remove the unreacted PU and homopolymers.

The surface morphologies of the microspheres were observed by a Zoom stereo optical microscope (ZSA302, Chongqing Optical & Electrical Instrument Co., Ltd.) and a scanning electron microscope (model S-3500 N, Hitachi, Japan).

We examined the swelling ratios (SRs) of the CaA and PU-*g*-CaA microspheres by weighing the samples under different pH conditions and calculated them with eq. (4):

$$\mathrm{SR}\ (\%) = (W_s - W_d)/W_d \times 100 \quad (4)$$

where W_s and W_d are the weights of the beads in the swollen and initial states, respectively.

RESULTS AND DISCUSSION

PU-*g*-SA was produced by free-radical polymerization, the mechanism of which is presented in Scheme 1. First, alginate was induced by the initiator, and macromolecular radicals were generated on the hydroxyl groups. Then, the radicals captured double-bond electrons on the macromonomer to form new macromolecular radicals. The chain polymerization proceeded to generate side chains, and PU-*g*-SA was obtained.

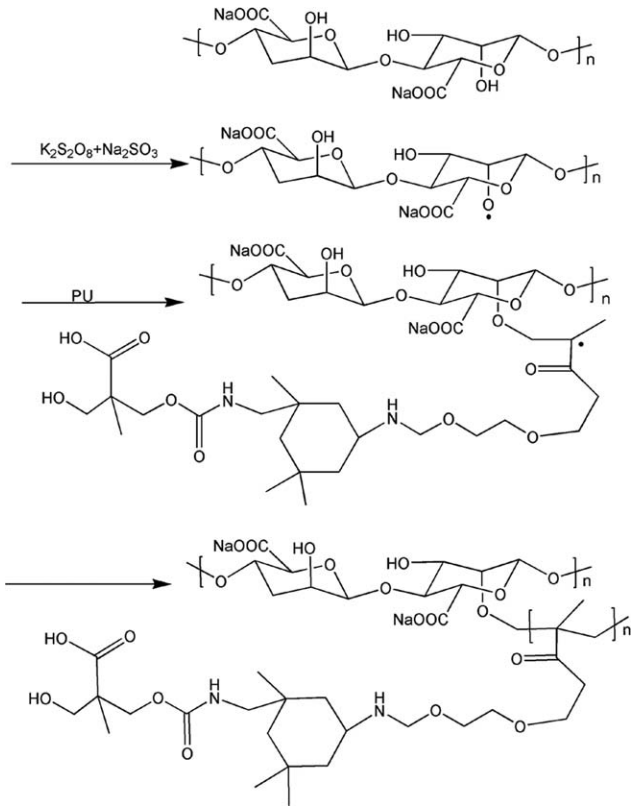

Scheme 1. Synthetic mechanism of PU-*g*-CaA.

FTIR Spectroscopy

FTIR spectra of the CaA, PU-*g*-CaA (with *G*% = 20%), and CaA–PU hybrid are shown in Figure 1(a). The stretching vibrations of the O—H bonds appeared in the range 3000–3600 cm^{-1}. The asymmetric and symmetric stretching vibrations of the CaA carboxylate group (—COO^-) were located at 1614 and 1427 cm^{-1}. The bands at 1030 and 941 were attributed to C—O stretching vibrations of the glucoside rings.[24] Compared with CaA, the spectrum of PU-*g*-CaA showed two new peaks at 1720 and 1246 cm^{-1}, which originated from the C=O and C—N stretching vibrations of secondary amide. The C—H stretching vibrations of alkyl groups on the PU side chains were around 2956 cm^{-1}. The ether bond generated in the grafting reaction possessed an absorption peak at 1130 cm^{-1}, which could not be found in the PU–CaA hybrid. In addition, in the spectrum of PU–CaA hybrid, the absorption bands at 3070, 1548, and 1410 cm^{-1} were assigned to CH_2=CR_2 on PU before the grafting reaction. Therefore, these results suggest that the PU segments were grafted onto CaA.

Solid-State NMR Spectroscopy

The ^{13}C-NMR spectra of CaA and PU-*g*-CaA are shown in Figure 1(b). The peak at 175 ppm was due to the carboxylic acid (—COOH) of alginate. The peaks of carbons on the glucoside ring of alginate are shown around 75 and 101 ppm. Compared with CaA, PU-*g*-CaA exhibited a new peak at 156 ppm due to the urethane carbon (—NHCOO). In addition, the peaks between 18 and 54 ppm were attributed to alkane carbons on

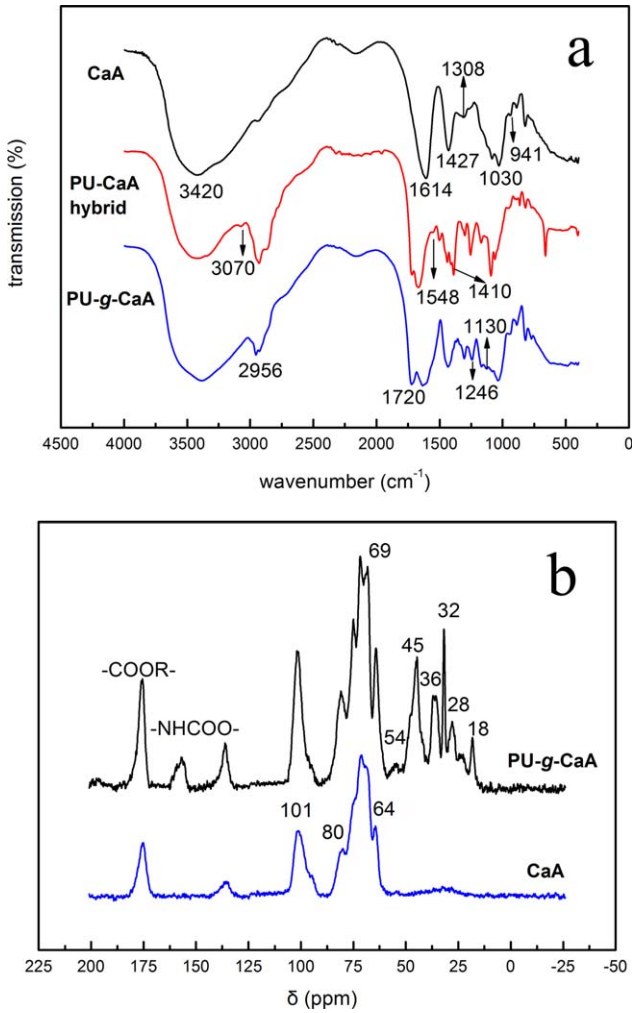

Figure 1. (a) FTIR and (b) ^{13}C-NMR spectra of hydrogel microspheres. [Color figure can be viewed in the online issue, which is available at wileyonlinelibrary.com.]

PU side chains. The peak at 69 ppm was ascribed to methylene carbon generated in the grafting reaction. These results of the ^{13}C-NMR spectra further prove that the grafting reaction had occurred.

Surface Morphology

Optical Microscopy. Optical micrographs of the hydrogel beads are presented in Figure 2. We observed that all of the beads appeared spherical with relatively smooth surfaces. This was because the surface crosslinking occurred immediately as the droplets of SA contacted the $CaCl_2$ solution.[25] In a comparison of Figures 2(b) and 2(d), we found that the CaA beads had better transparency than PU-*g*-CaA. After modification, the components of the beads became complicated, and a partial crystallizing region was introduced.[23] As a result, the transparency decreased, and numerous spots with white [Figure 2(a)] or black [Figure 2(b)] appearances were observed in the photographs.

Scanning Electron Microscopy. Scanning electron microscopy was used to explore the micromorphology of the polymer

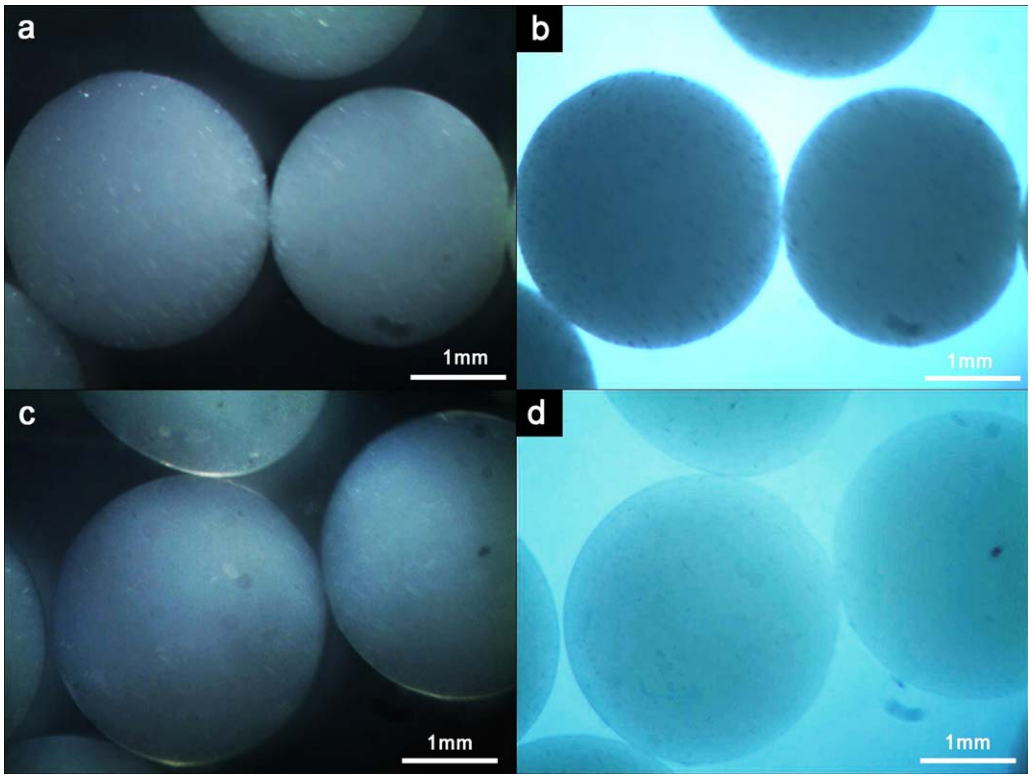

Figure 2. Optical micrographs of the PU-*g*-CaA beads under (a) reflecting and (b) transmitting light sources and CaA beads under (c) reflecting and (d) transmitting light sources. [Color figure can be viewed in the online issue, which is available at wileyonlinelibrary.com.]

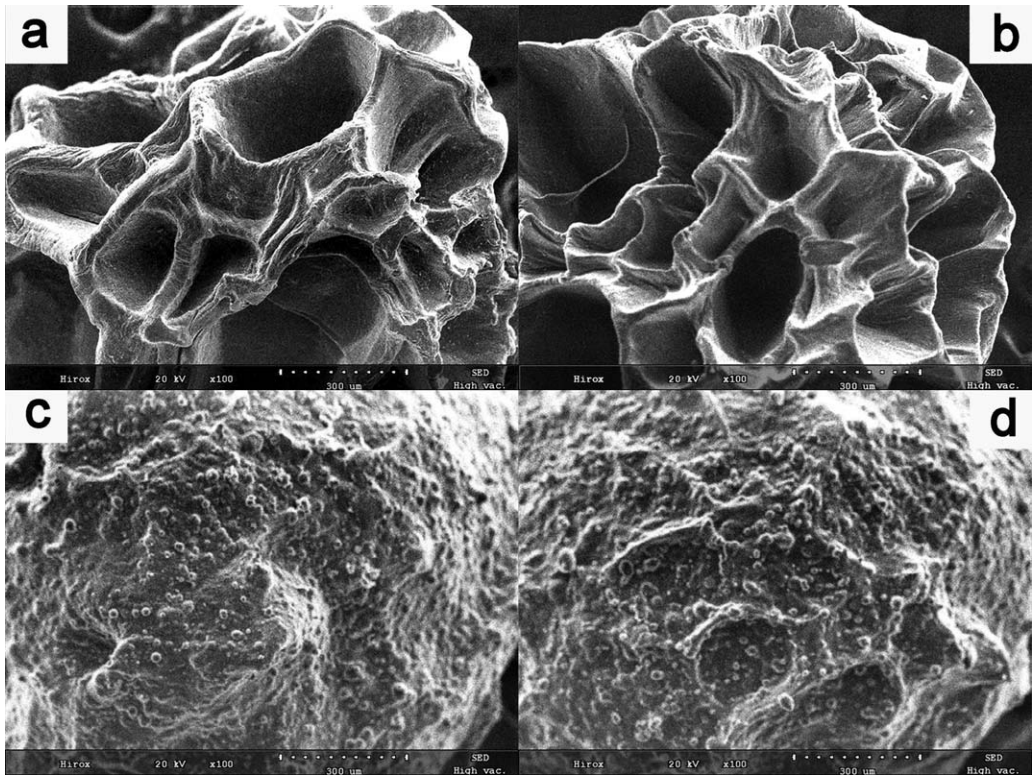

Figure 3. Electron micrographs of the (a) CaA MIPs, (b) CaA NIPs, (c) PU-*g*-CaA MIPs, and (d) PU-*g*-CaA NIPs after freeze-drying.

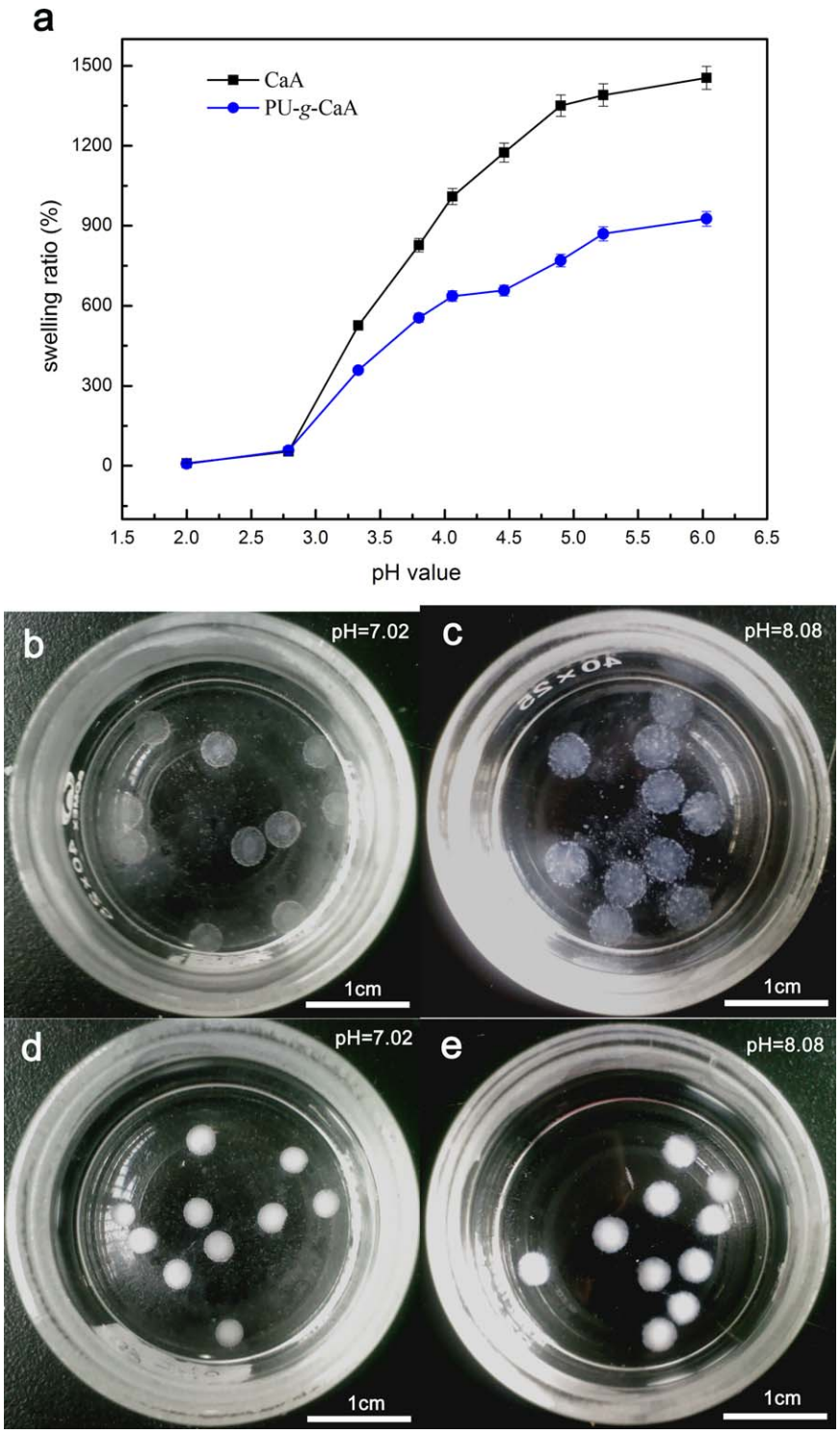

Figure 4. (a) SRs and optical photographs of the (b,c) swollen CaA beads and (d,e) PU-*g*-CaA beads in different pH media. [Color figure can be viewed in the online issue, which is available at wileyonlinelibrary.com.]

beads, as shown in Figure 3. Both of the CaA samples with and without protein template [Figure 3(a,b)] became more hollow and less spherical after freeze-drying. This was because the hydrogel walls of the pores collapsed during freeze-drying, and this eliminated bound moisture. The surface of the CaA beads appeared to have a bordered, craterlike frame, and the inner surface of the wall was generally smooth. The PU-*g*-CaA beads with and without protein template [Figure 3(c,d)] exhibited relatively better sphericity after freeze-drying, and this indicated that the mechanical strength of the PU-*g*-CaA beads was improved. The physical crosslinking formed by the grafted PU side chains was strong enough to support the hydrogel matrix

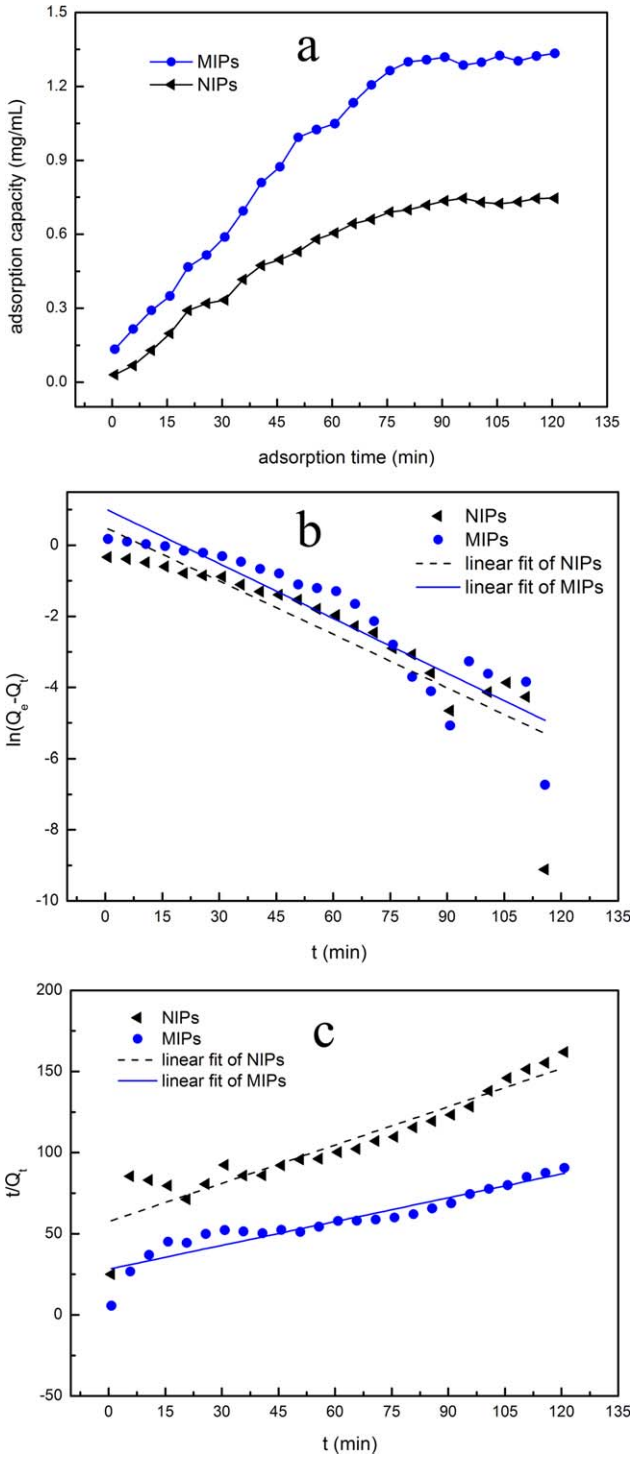

Figure 5. Adsorption kinetics of the (a) PU-*g*-CaA microspheres, (b) PFO model, and (c) PSO model for the adsorption of BSA onto PU-*g*-CaA microspheres. [Color figure can be viewed in the online issue, which is available at wileyonlinelibrary.com.]

as water was eliminated; therefore, no hollowness was generated. In addition, the morphology of the PU-*g*-CaA beads obviously differed from that of the CaA samples by the rougher surface with a protuberance. This was because of the aggregation of the grafted hydrophobic PU segments.

Table I. Parameters Obtained for the Kinetic Models and Experiments

Model	Microspheres	R^2	k	$Q_{e,cal}$	$Q_{e,exp}$
PFO	MIPs	0.8517	0.0515	2.7946	1.32
	NIPs	0.7626	0.05	1.6458	0.75
PSO	MIPs	0.8778	0.0085	2.0454	1.32
	NIPs	0.8770	0.0108	1.2704	0.75

In a comparison of the images of the MIPs [Figure 3(a,c)] and NIPs [Figure 3(b,d)], no significant morphology differences were observed between the samples with and without template. Therefore, doubt could be eliminated that protein might have acted as a pore-forming agent and that this might have led to unexpected porous surface adsorption.

Swelling Behaviors

In the study of swelling behavior, samples were chosen with a grafting ratio of 20%, which was proven to be the optimum value for IE and adsorption capacity in previous studies.[26] The SRs of the polymer beads according to pH were characterized, and the results are shown in Figure 4(a). The SRs of all of the samples were lowered because the buffer solution pH was less than 3.0, and it grew along with the increase of pH. The results were attributed to the fact that most of the —COO^- groups of CaA were transformed into —COOH rather than $(—COO)_2Ca$ at low pH.[27,28] The intermolecular hydrogen bonds were formed between the carboxylate groups of CaA predominating over the polymer–H_2O interactions. Therefore, the swelling behavior was hindered. However, as the pH increased, most of the —COOH groups tended to dissociate into —COO^-; this led to electrostatic repulsion between the polymer chains. Furthermore, the osmotic pressure also increased inside the beads because of the high concentration of free H^+.[28] As a result, water molecules diffused into the hydrogel beads more easily, and this resulted in a high SR. The swelling behavior of the PU-*g*-CaA samples was similar to that of the CaA beads, except for a lower SR. This was because the grafted PU side chains were hydrophobic and reduced the water permeability.

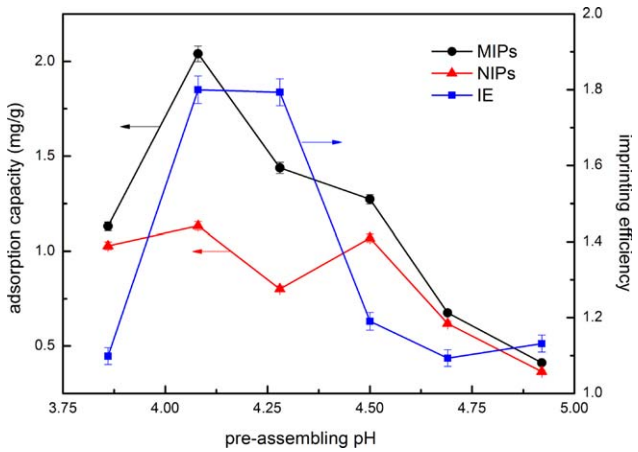

Figure 6. Adsorption capacity and IE of the PU-*g*-CaA beads at different preassembly pH values. [Color figure can be viewed in the online issue, which is available at wileyonlinelibrary.com.]

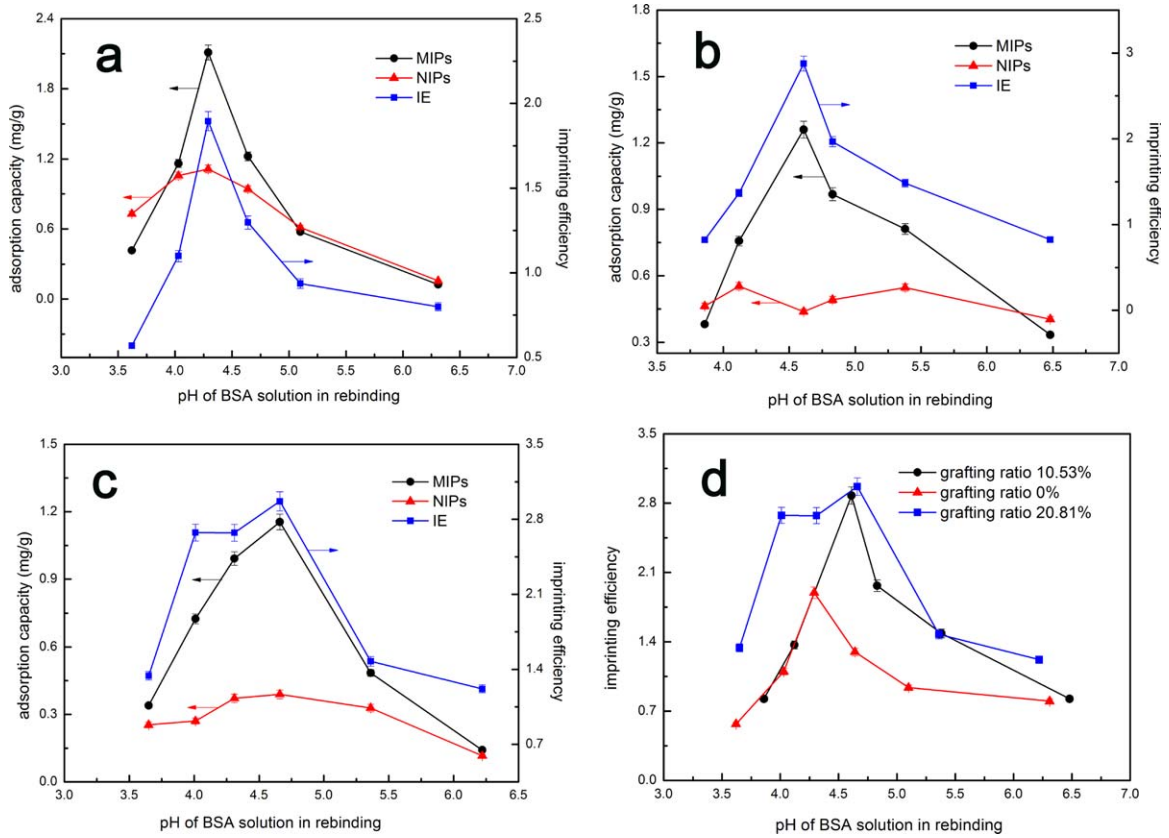

Figure 7. Adsorption capacity and IE of the hydrogel beads at different rebinding pH values: (a) CaA beads, (b) PU-*g*-CaA beads with a grafting ratio of 10.53%, and (c) PU-*g*-CaA beads with a grafting ratio of 20.81%. (d) Imprinting efficiencies of the different beads. [Color figure can be viewed in the online issue, which is available at wileyonlinelibrary.com.]

The optical photos of the swollen CaA [Figure 4(b,c)] and PU-*g*-CaA [Figure 4(d,e)] beads in basic solutions are also shown in Figure 4. Both of the samples were found to be swollen in the environment at pHs of greater than 7.0, whereas the modified beads exhibited more opacification than the CaA samples. The difference was ascribed to the PU side chains, which provided partial crystallization zones formed by chain entanglement.[23] When immersed in a solution at pH 8.08, the CaA beads were disintegrated by surface erosion, and this made accurate weighing of the swollen microspheres more difficult.

Adsorption Behavior of the PU-*g*-CaA Beads

The protein rebinding kinetics of the PU-*g*-CaA microspheres are presented in Figure 5. As shown in Figure 5(a), the rebinding rate of the MIPs was higher than that of the NIPs. This was due to the presence of a large amount of specific and unoccupied binding sites in the microspheres. The rebinding reached equilibrium within about 120 min. The adsorption capacities were 1.32 mg/g for the MIPs and 0.75 mg/g for the NIPs.

Figure 5(b,c) shows the pseudo-first-order (PFO) and pseudo-second-order (PSO) kinetics for the adsorption of BSA onto the

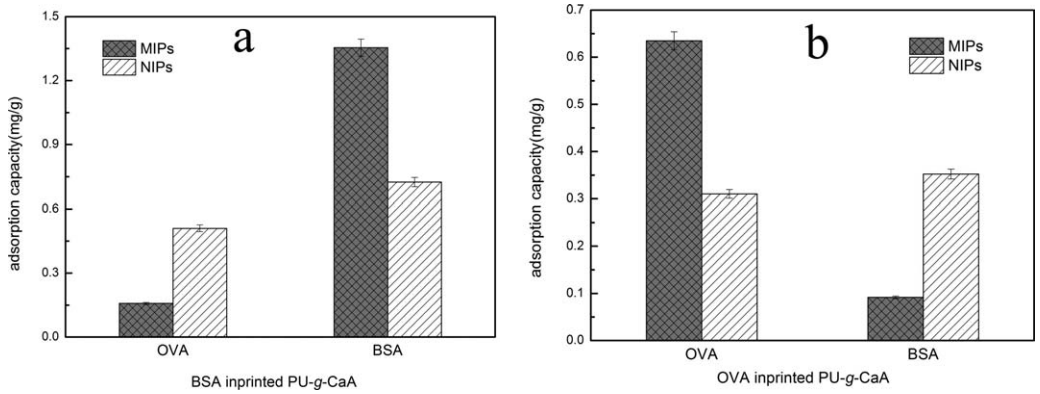

Figure 8. Selectivities of the (a) BSA-imprinted PU-*g*-CaA and (b) OVA-imprinted PU-*g*-CaA.

PU-*g*-CA microspheres. These two kinetic models could be expressed in linear forms as follows:[29]

$$\ln(Q_e - Q_t) = \ln Q_e - k_1 t \quad (5)$$

$$t/Q_t = t/Q_e + 1/k_2 Q_e^2 \quad (6)$$

where Q_e and Q_t represent the amounts of BSA adsorbed at equilibrium and any time (m/g), respectively, and k_1 (min^{-1}) and k_2 (g mg^{-1} min^{-1}) are the rate constants of the PFO and PsSO models, respectively, t is the adsorption time (min).

The values of the correlation coefficients (R^2's), rate constant (k), calculated amount of BSA adsorbed at equilibrium ($Q_{e,cal}$), and experimental amount of BSA adsorbed at equilibrium ($Q_{e,exp}$) are listed in Table I. Compared with the PFO model, the adsorption process fit the PSO models better. However, we observed that the $Q_{e,cal}$ values were different from the $Q_{e,exp}$ values and the R^2 values were lower than 0.9. The result suggests that neither of the two models matched well with the experimental adsorption behaviors of the PU-*g*-CaA microspheres. Protein adsorption on PU-*g*-CaA probably followed a more suitable model other than PFO or PSO.

Adsorption Capacity and IE of the MIPs with Different Preassembly pH Values

The configurations of the protein template and imprinted matrix were remarkably affected by the environmental H^+ and other ions. Therefore, the rebinding behavior was closely related to the pH where the polymer preassembled and gelated. The grafted samples were prepared with a grafting ratio of 20%, as has been proven to be beneficial for imprinting.[26] The different preassembly pH were adjusted by adding 0.1 mol/L hydrochloride solution during the preparation of the protein-imprinted microspheres. The adsorption capacities and IE were measured, and the results are shown in Figure 6. We found that the equilibrium adsorption capacity (ca. 2.03 mg/g) and IE (ca. 1.80) were obtained when the pH value was near 4.1. Both the BSA and alginate were negatively charged when the environmental pH was above 4.7. Therefore, the interaction between BSA and the hydrogel matrix was weakened in the preassembling systems with higher pHs. As a result, the accuracy of imprinting sites was deteriorated, and no remarkable specific adsorption was observed. When the pH value was 4.1, the BSA templates were positively charged, and the preassembling of BSA and hydrogel groups was facilitated. However, when the pH decreased to lower than 4.0, the preassembling was obstructed again, and samples with almost no specific recognition were generated. This was due to the fact that the pK_a values of the mannuronic and guluronic acid groups of alginate were 4.0 and 3.2, respectively.[30] As a result, gelation occurred in the alginate solution when the pH was lower than 4.0. Under this condition, the alginate solution exerts more resistance to protein diffusion, and this was disadvantageous for the production of imprinting sites.

Adsorption Capacity and IE of MIPs with Different Rebinding pH

The pH value of the rebinding solution is one of the most important parameters in the adsorption process because proteins are charged differently in three-dimensional structures as the pH varies.[31] The effect of the rebinding pH on the BSA adsorption capacity was investigated for the MIPs and NIPs with different grafting ratios, as shown in Figure 7. It was revealed that the capacity of BSA adsorption depended significantly on the pH value. The greatest adsorption capacities of the imprinted samples were observed (2.11, 1.26, and 1.15 mg/g for of grafting ratios 0, 10.53, and 20.81%, respectively) when the pH value was between 4.2 and 4.7. Lowered adsorption capacities were obtained when the pH was less than 4.2 or greater than 4.7. This was due to the pI of BSA (4.7). When the surrounding pH was between 4.2 and 4.7, the BSA target was neutral, and the hydrophobic interaction between the BSA and beads was maximized.[32,33] However, in solutions with pH values of less than 4.2 or greater than 4.7, the variations in the protein conformation and charge caused a decrease in the BSA adsorption amount.

These adsorption behaviors were also confirmed by the swelling behaviors, as was mentioned in the Swelling Behaviors section. It has been documented that an optimum swelling state is required for the best specific rebinding.[34] In a medium with a pH of less than 4.2, the lowered SR of the beads hindered protein inward diffusion and rebinding. However, in a medium with a pH of greater than 4.7, the microspheres possessed an excessively high SR and even disintegrated. The imprinted cavities were deformed, and this was also disadvantageous for the rebinding of the target protein. Around pH 4.2–4.7, the hydrogel matrix was swollen to the most appropriate state.

As shown in Figure 7(d), we found that the influence of pH on IE was similar to that on the adsorption capacity. The highest IEs (1.89, 2.87, and 2.97 for grafting ratios of 0, 10.53, and 20.81%, respectively) were approached at appropriate pH when the imprinting structure remained unchanged. Furthermore, with increasing grafting ratio, the IE curves were found to be generally increased throughout the whole pH span. This was because the grafting side chains improved the mechanical and swelling properties of the microspheres. The molecular imprints generated in the modified alginate hydrogels were, therefore, preserved. When the grafting ratio increased, more accessible and stable imprinting sites were constructed, as has been documented previously.[26]

Recognition Properties

The adsorption capacities of BSA and OVA for different hydrogel microspheres are shown in Figure 8. We observed that the MIPs with BSA or OVA imprints possessed relatively higher adsorption capacities than their respective template proteins, whereas for competitive proteins, the adsorption capacities were remarkably lowered. We ascribed this to the formation of smaller cavities with unique and more specific shape memory, which would no longer be available for other proteins. For the template proteins, the adsorption capacities of the MIPs were higher than those of the NIPs. This was attributed to the imprinting sites of the MIPs, which facilitated specific recognition. The selectivities of the PU-*g*-CaA MIPs (8.08 for BSA imprinting and 7.23 for OVA imprinting) were higher than in previous studies.[34] This further demonstrated that the introduction of PU chains was beneficial for specific recognition.

CONCLUSIONS

PU-*g*-CaA was synthesized and used for the preparation of BSA-imprinted hydrogels. The PU-*g*-CaA microspheres exhibited a more rough and dense surface than the CaA samples. A high absorption capacity and IE of the MIPs were obtained (ca. 2.03 mg/g and 1.80, respectively) when the preassembly pH was around 4.1 and rebinding pH was around 4.6. The introduction of PU side chains was beneficial for the specific recognition of protein, and this was confirmed by the improvement of the selectivity. The reason for the previous results was that hydrophobic segments and physical crosslinking points were formed by PU side-chain entanglement. This suggested that the protein-imprinted PU-*g*-CaA hydrogel is a promising material for the design of protein-selective detection, quantification, and separation devices.

ACKNOWLEDGMENTS

The authors thank the China Postdoctoral Science Foundation (contract grant number 2012M511439) and the Fuzhou University Science and Technology Development Fund (contract grant number 2014-XQ-23) for their support.

REFERENCES

1. Yang, K.; Zhang, L.; Liang, Z.; Zhang, Y. *Anal. Bioanal. Chem.* **2012**, *403*, 2173.
2. Sunayama, H.; Ooya, T.; Takeuchi, T. *Chem. Commun.* **2014**, *50*, 1347.
3. Haupt, K.; Linares, A. V.; Bompart, M.; Bui, B. T. *Top. Curr. Chem.* **2012**, *325*, 1.
4. Moreira, F. T. C.; Sharma, S.; Dutra, R. A. F.; Noronha, J. P. C.; Cass, A. E. G.; Sales, M. G. F. *Sens. Actuators B* **2014**, *196*, 123.
5. Zhang, M.; Huang, J.; Yu, P.; Chen, X. *Talanta* **2010**, *81*, 162.
6. Zayats, M.; Kanwar, M.; Ostermeier, M.; Searson, P. C. *Macromolecules* **2011**, *44*, 3966.
7. Zdyrko, B.; Hoy, O.; Luzinov, I. *Biointerphases* **2009**, *4*, 17.
8. Asliyuce, S.; Uzun, L.; Rad, A. Y.; Unal, S.; Say, R.; Denizli, A. *J. Chromatogr. B* **2012**, *889*, 95.
9. Feng, H.; Mao, X.; Chu, B.; Xie, C. *J. Appl. Polym. Sci.* **2014**, 131.
10. El Kirat, K.; Bartkowski, M.; Haupt, K. *Biosens. Bioelectron.* **2009**, *24*, 2618.
11. Takátsy, A.; Végvári, Á.; Hjertén, S.; Kilár, F. *Electrophoresis* **2007**, *28*, 2345.
12. Adrus, N.; Ulbricht, M. *Polymer* **2012**, *53*, 4359.
13. Vaihinger, D.; Landfester, K.; Kräuter, I.; Brunner, H.; Tovar, G. E. M. *Macromol. Chem. Phys.* **2002**, *203*, 1965.
14. Lin, Y.; Tang, S.; Mao, X.; Bao, L. *J. Biomed. Mater. Res. A* **2008**, *85*, 573.
15. Zhao, K.; Cheng, G.; Huang, J.; Ying, X. *React. Funct. Polym.* **2008**, *68*, 732.
16. Xia, Y.-Q.; Guo, T.-Y.; Song, M.-D.; Zhang, B.-H.; Zhang, B.-L. *React. Funct. Polym.* **2006**, *66*, 1734.
17. Zhang, F.; Cheng, G.; Ying, X. *React. Funct. Polym.* **2006**, *66*, 712.
18. Herrero, E. P.; Martín Del Valle, E. M.; Peppas, N. A. *Ind. Eng. Chem. Res.* **2010**, *49*, 9811.
19. Bayer, C. L.; Herrero, E. P.; Peppas, N. A. *J. Biomater. Sci. Polym. Ed.* **2011**, *22*, 1523.
20. Zhao, K.; Cheng, G.; Wei, J.; Zhou, J.; Zhang, J.; Chen, L. *Macromol. Symp.* **2010**, 126.
21. Ying, X.; Zhang, F.; Zhang, L.; Cheng, G. *J. Appl. Polym. Sci.* **2010**, *115*, 3516.
22. Kim, J.-S.; Pathak, T. S.; Yun, J.-H.; Kim, K.-P.; Park, T.-J.; Kim, Y.; Paeng, K.-J. *J. Polym. Environ.* **2012**, *21*, 224.
23. Wang, J.; Ying, X.; Li, X.; Zhang, W. *Mater. Lett.* **2014**, *126*, 263.
24. Daemi, H.; Barikani, M.; Barmar, M. *Carbohydr. Polym.* **2013**, *92*, 490.
25. Pillay, V.; Fassihi, R. *J. Controlled Release* **1999**, *59*, 243.
26. Li, L.; Ying, X.; Liu, J.; Li, X.; Zhang, W. *Mater. Lett.* **2015**, *143*, 248.
27. Li, H.; Li, X.-Y. *J. Fiber Bioeng. Inform.* **2009**, *2*, 168.
28. Abd El-Ghaffar, M. A.; Hashem, M. S.; El-Awady, M. K.; Rabie, A. M. *Carbohydr. Polym.* **2012**, *89*, 667.
29. Fu, J.; Chen, Z.; Wang, M.; Liu, S.; Zhang, J.; Zhang, J.; Han, R.; Xu, Q. *Chem. Eng. J.* **2015**, *259*, 53.
30. Kaygusuz, H.; Erim, F. B. *React. Funct. Polym.* **2013**, *73*, 1420.
31. Demirel, G.; Özçetin, G.; Turan, E.; Çaykara, T. *Macromol. Biosci.* **2005**, *5*, 1032.
32. Zhang, Z.; Yang, X.; Chen, X.; Zhang, M.; Luo, L.; Peng, M.; Yao, S. *Anal. Bioanal. Chem.* **2011**, *401*, 2855.
33. Tang, P.-P.; Cai, J.-B.; Su, Q.-D. *Chin. J. Chem. Phys.* **2010**, *23*, 195.
34. Ying, X.; Qi, L.; Li, X.; Zhang, W.; Cheng, G. *J. Appl. Polym. Sci.* **2013**, *127*, 3898.